

Evaporation residue excitation function and spin distribution for $^{31}\text{P} + ^{170}\text{Er}$

G. Mohanto,^{*} N. Madhavan, S. Nath, J. Gehlot, Ish Mukul, A. Jhingan, T. Varughese, A. Roy, and R. K. Bhowmik
Inter University Accelerator Centre, Aruna Asaf Ali Marg, New Delhi 110067, India

I. Mazumdar, D. A. Gothe, and P. B. Chavan
Tata Institute of Fundamental Research, Homi Bhabha Road, Mumbai 400005, India

J. Sadhukhan
Department of Physics and Astrophysics, University of Tennessee, Knoxville, Tennessee 37996, USA
and Physics Division, Oak Ridge National Laboratory, Oak Ridge, Tennessee 37831, USA

S. Pal[†]
CS-6/1, Golf Green, Kolkata 700095, India

Maninder Kaur and Varinderjit Singh
Department of Physics, Panjab University, Chandigarh 160014, India

A. K. Sinha
UGC-DAE CSR, Kolkata Centre, 3/LB-8, Bidhan Nagar, Kolkata 700098, India

V. S. Ramamurthy
National Institute of Advanced Studies, Indian Institute of Science Campus, Bangalore 560012, India
 (Received 17 August 2013; published 19 September 2013)

Background: Synthesis of a doubly magic spherical nucleus beyond $^{208}_{82}\text{Pb}_{126}$ is a key question in contemporary nuclear physics. Such nuclei can exist solely because of shell stabilization. As the formation cross section of super heavy elements is prohibitively low, attempts have been made to understand stabilizing effects of closed proton (Z) and neutron (N) shells in the vicinity of $^{208}_{82}\text{Pb}_{126}$.

Purpose: The present work attempts to elucidate the stabilizing effect of shell closure, in general, and the same of $Z = 82$, in particular.

Methods: The evaporation residue (ER) excitation function and ER-gated γ -multiplicity distribution have been measured for the reaction $^{31}\text{P} + ^{170}\text{Er}$ at a laboratory energy range of 134–172 MeV. The measurements have been carried out using the HYbrid Recoil mass Analyzer (HYRA) in gas-filled mode and a 4π spin spectrometer consisting of 29 NaI(Tl) detectors. Results of the present reaction have been compared with those of the reaction $^{30}\text{Si} + ^{170}\text{Er}$. Statistical model calculation has been performed for both the systems.

Results: The two reactions, induced by ^{30}Si and ^{31}P projectiles, resulted in compound nuclei (CN) ^{200}Pb ($Z = 82$) and ^{201}Bi ($Z = 83$), respectively. To reproduce experimental ER cross sections, the liquid drop fission barrier (B_f) had to be scaled in the statistical model calculation. The scaling factor (K_f) varies from 0.75 to 1.05 and 0.90 to 1.05 for ^{30}Si and ^{31}P induced reactions, respectively. No significant differences have been found between γ -multiplicity distribution and the distribution moments of the two systems.

Conclusions: No clear signature has been observed in favor of extra stability of the ERs with closed proton shell ($Z = 82$) as K_f values of the two systems match within errors. More exclusive measurements and comparison between more systems forming CN/ER around $Z = 82$ are desirable.

DOI: [10.1103/PhysRevC.88.034606](https://doi.org/10.1103/PhysRevC.88.034606)

PACS number(s): 25.70.Jj, 24.60.Dr

I. INTRODUCTION

In recent years, one great concern of experimental heavy-ion physics is the formation of super heavy elements (SHE). Early theoretical works (e.g., Ref. [1]) predicted that the next doubly shell-closed spherical nucleus, after $Z = 82$ and $N = 126$, would exist at $Z = 114$ and $N = 184$. Nuclei in the vicinity of these N and Z values are expected to be

comparatively stable because of the shell correction energy. A few SHE nuclei have already been synthesized experimentally and the search for more such nuclei is going on. Of late, there are different predictions about the exact Z and N where the next shell closure might occur [2,3]. Many efforts are being made to find the values experimentally, which will help in obtaining more accurate theoretical model parameters. The main difficulty in forming a nucleus in the SHE region is their extremely low production rate (cross section \sim pb). Fast-fission, quasifission, and fusion-fission are the hurdles that prevent formation of evaporation residues (ERs) in this region. These processes make the experiments time consuming

^{*}gayatrimohanto@gmail.com

[†]Formerly with Variable Energy Cyclotron Centre, Kolkata, India.

and selection of target-projectile combination plays a crucial role in such experiments.

Whether shell closure plays any role in the reaction dynamics is an important question to settle while studying reactions in heavy and super heavy regions. Shell closure of either of the reaction partners was observed in some cases to affect the fusion-fission dynamics [4]. Srivastava *et al.* [5] observed that $N = 126$ shell closure of the compound nuclei (CN) gave rise to an enhanced fission fragment angular anisotropy. A similar effect was also observed by Mahata *et al.* [6]. There are not many reports on the effect of proton shell closure of the CN in the literature. Nath *et al.* [7] reported a systematic study of ^{19}F -induced reactions leading to CN ^{194}Hg , ^{200}Pb , ^{203}Bi , and ^{205}At . The fission barrier for the system leading to CN with $Z = 82$ was found to deviate from the systematic (N, Z) dependence. It may however be pointed out here that the shell closure effects at $N = 126$ or $Z = 82$ are expected to be significantly different from those of the super heavy nuclei because while the liquid drop model accounts for a reasonable part of the fission barriers of the nuclei with $Z = 82$ or $N = 126$, the fission barriers of super heavy nuclei arise entirely due to shell effects.

We intend to study the effect of proton shell closure of CN on fusion-fission dynamics in the vicinity of $^{208}\text{Pb}_{126}$. Observation of ER is a sure signature of CN formation and ER-gated spin distribution can give information about the partial waves which contribute to ER formation (in other words, ℓ values that survive fission). In this article, we report the measurements of ER cross sections (σ_{ER}) and ER-gated γ multiplicity distributions for the system $^{31}\text{P} + ^{170}\text{Er}$. Then we compare the results with that of the reaction $^{30}\text{Si} + ^{170}\text{Er}$. These two reactions form CN ^{201}Bi and ^{200}Pb , respectively. Both CN have the same number of neutrons ($N = 118$) but ^{200}Pb has proton shell closure with $Z = 82$ while ^{201}Bi has one extra proton beyond closed shell ($Z = 83$).

II. EXPERIMENTAL DETAILS

The experiments were carried out at IUAC, New Delhi, using beams of ^{30}Si and ^{31}P , delivered from the 15UD Pelletron + LINAC facility. A target of enriched ^{170}Er (more than 97% enrichment) of thickness $130 \mu\text{g}/\text{cm}^2$ [8], sandwiched between two carbon layers of thickness 45 (upstream) and 23 (downstream) $\mu\text{g}/\text{cm}^2$, was prepared using the vacuum evaporation technique. σ_{ER} and ER-gated γ -multiplicity distributions were measured for the reaction $^{31}\text{P} + ^{170}\text{Er}$ at laboratory energy (E_{lab}) = 134.4, 136.5, 141.6, 146.7, 151.9, 157.0, 162.1, 167.3, 172.0, 177.2 MeV, having average beam current 0.5 pA. A schematic diagram of the experimental setup is shown in Fig. 1.

ERs were separated from the intense beam background with the help of the HYbrid Recoil mass Analyzer (HYRA) [9], which is a dual-mode, dual-stage recoil separator. In the present study, the first stage of the HYRA, having electromagnetic configuration Q1Q2-MD1-Q3-MD2-Q4Q5 (Q and MD stand for magnetic quadrupole and magnetic dipole, respectively), was used in gas-filled mode. The main advantage of a gas-filled recoil separator is its enhanced transmission

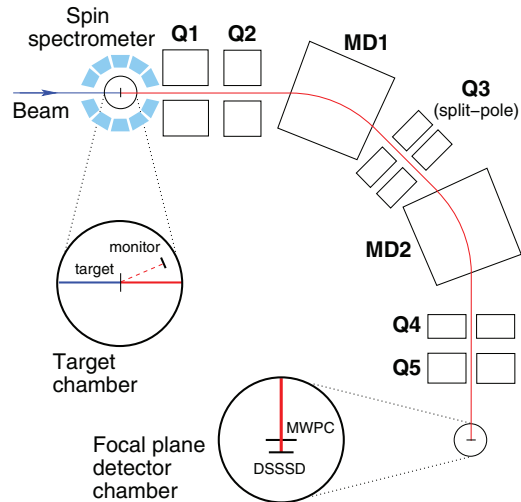


FIG. 1. (Color online) Schematic diagram of the experimental setup used for measuring ER cross sections and ER-gated spin distributions.

efficiency (ϵ), which is achieved because of velocity and charge state focusing of the transmitted ions. The HYRA was filled with helium and the pressure was varied to get optimum ϵ at 0.15 Torr. The gas-filled region of the HYRA was separated from the beam line, maintained at high vacuum, by a $1.3 \text{ mg}/\text{cm}^2$ thick nickel window foil, placed at a distance of 34 cm upstream from the target position. Magnetic fields for all the ion optical elements were calculated using a simulation code [10]. At each E_{lab} , magnetic fields were scanned in a range of $\pm 10\%$ of the calculated values. For most cases, calculated values were found to be the optimum ones.

γ rays from ERs were detected using a spin spectrometer [11,12], placed around the target chamber and consisting of 32 NaI(Tl) detectors, which subtended a solid angle of $\sim 4\pi$ sr. In the present study, two detectors were removed for beam entry and exit and one was removed for positioning the target ladder. The remaining 29 detectors yielded a solid angle coverage of $\sim 91\%$ of 4π sr. The compact design of the 4π detector array restricted the inner radius of the target chamber to only 6 cm. A monitor detector was placed inside the chamber to record Rutherford-scattered beam particles at an angle of 25.9° with respect to the beam direction and at a distance of 2.3 cm from the target. The small opening of the chamber limited angular acceptance of the HYRA to polar angle 3.4° . The beam was centered on the target by maximizing beam current at a beam catcher placed behind MD1.

ERs were detected at the focal plane with the help of a multiwire proportional counter (MWPC) of area $5 \times 15 \text{ cm}^2$. A double-sided silicon strip detector (DSSSD), with 16 strips on each side and area $5 \times 5 \text{ cm}^2$, was placed behind the MWPC. These two detectors recorded energy loss (ΔE) and residual energy (E_{res}) of the ERs, respectively. A time-of-flight (TOF) spectrum was generated with the timing pulse from the MWPC anode as start and the radio frequency (RF) signal, delayed suitably, as stop. Separation between consecutive RF pulses was $2 \mu\text{s}$. The ΔE vs TOF and the ΔE vs E_{res} spectra helped in unambiguous identification of ERs from $^{31}\text{P} + ^{170}\text{Er}$. Figure 2

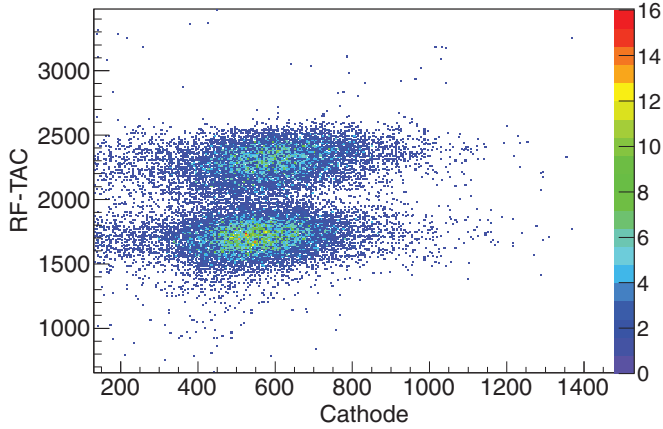


FIG. 2. (Color online) ΔE vs TOF spectrum for $^{31}\text{P} + ^{170}\text{Er}$ at $E_{\text{lab}} = 134.4$ MeV. The group of particles at the bottom are ERs from this reaction. The other group at the top resulted from contamination of $^{\text{nat}}\text{Ba}$ in the target. See text for details.

shows ΔE vs TOF plot at $E_{\text{lab}} = 134.4$ MeV. Two groups of particles with overlapping ΔE but different TOF are clearly distinguishable. The group of particles at the top are ERs resulting from fusion of ^{31}P with $^{\text{nat}}\text{Ba}$, present in the target as a contaminant. Its presence was confirmed by characterizing the target using Rutherford back scattering (RBS) [8]. Although the amount of $^{\text{nat}}\text{Ba}$ in the target was less than 1% of ^{170}Er , the population of the two groups of ERs in the ΔE vs TOF spectrum was comparable because of much higher fusion cross section for $^{31}\text{P} + ^{\text{nat}}\text{Ba}$ than the same for $^{31}\text{P} + ^{170}\text{Er}$. Over the range of E_{lab} used in this study, the two groups of ERs could be clearly separated though their relative population varied.

III. EXPERIMENTAL DATA ANALYSIS

A. ER excitation function

Total ER cross sections were calculated using the relation

$$\sigma_{\text{ER}} = \frac{Y_{\text{ER}}}{Y_{\text{Mon}}} \left(\frac{d\sigma}{d\Omega} \right)_{\text{Ruth}} \Omega_{\text{Mon}} \frac{1}{\epsilon_{\text{HYRA}}}, \quad (1)$$

where Y_{ER} is ER yield at the focal plane, Y_{Mon} is the yield of elastically scattered projectiles registered by the monitor detector, $(\frac{d\sigma}{d\Omega})_{\text{Ruth}}$ is the differential Rutherford scattering cross section, Ω_{Mon} is the solid angle subtended by the monitor detector, and ϵ_{HYRA} is the transmission efficiency of the HYRA. ϵ_{HYRA} is defined by the ratio of ERs detected at the focal plane to the total number of ERs produced in the target. This quantity depends on [7] entrance channel mass asymmetry, beam energy, target thickness, exit channels to be studied, angular acceptance of the HYRA, gas pressure, magnetic field settings of the HYRA, and active area of the focal plane detector. The conventional method of experimentally finding ϵ of a recoil separator is to detect γ rays from ERs in singles and in coincidence with ERs and then taking the ratio of counts of a specific γ ray from both the spectra. But in the present case, this method could not be used because of the large background of γ rays originating from the thick nickel window foil in the singles spectrum. We estimated ϵ_{HYRA} by

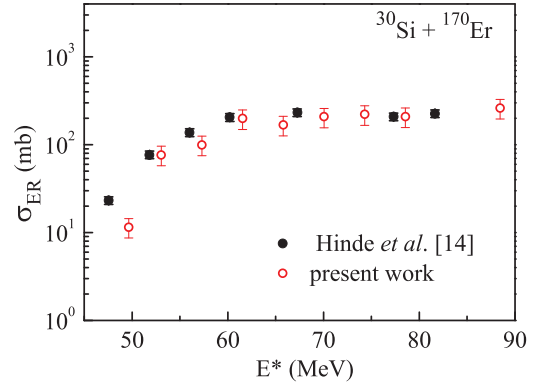


FIG. 3. (Color online) Measured σ_{ER} for the system $^{30}\text{Si} + ^{170}\text{Er}$ as a function of E^* . σ_{ER} taken from Ref. [14] are also shown.

a method, first used in Ref. [13], in which a similar reaction, namely $^{30}\text{Si} + ^{170}\text{Er}$, was used as the reference. σ_{ER} for this reaction had been available in the literature [14].

In an earlier experiment, we measured the ER-gated γ -multiplicity distribution for $^{30}\text{Si} + ^{170}\text{Er}$ at different E_{lab} . First, we calculated ϵ_{HYRA} for this reaction at a particular E_{lab} from Eq. (1), taking σ_{ER} from Ref. [14]. ϵ_{HYRA} is expected to vary over the range of E_{lab} because of various factors, as has been mentioned earlier. The most dominant of these factors is the ER angular distribution in the case of a gas-filled separator. ER angular distributions were calculated at each E_{lab} using the semimicroscopic Monte Carlo code TERS [15]. The distributions were then compared within the angular acceptance of the HYRA and correction factors were worked out to get ϵ_{HYRA} at all other E_{lab} . This new set of ϵ_{HYRA} was used to calculate σ_{ER} for $^{30}\text{Si} + ^{170}\text{Er}$. Those are shown in Fig. 3 along with σ_{ER} from Ref. [14]. The two sets are in agreement with each other except for a single E_{lab} below the Coulomb barrier (V_B).

Since the present reaction, $^{31}\text{P} + ^{170}\text{Er}$, is very similar to the reference reaction, ϵ_{HYRA} for the same was obtained from ϵ_{HYRA} for the reference reaction, after correcting for differences in angular distributions (see Fig. 4) at each E_{lab} . Figure 5 shows σ_{ER} as a function of excitation energy (E^*) for the system $^{31}\text{P} + ^{170}\text{Er}$. The cross sections are quoted with both systematic and statistical errors and the dominant contributor is the uncertainty ($\sim 15\%$) in the estimation of ϵ_{HYRA} .

B. ER-gated spin distribution

ER-gated spin distributions for the system $^{31}\text{P} + ^{170}\text{Er}$ were extracted from the experimental ER-gated γ -fold distributions. The method of conversion from γ -fold distribution to γ -multiplicity distribution and further to the corresponding spin distributions was explained in detail in Ref. [16]. If M uncorrelated γ rays are emitted and are detected using an array of N detectors, then the probability of firing p detectors will be given by $R(p, M)$. The response function $R(p, M)$ was calculated using the iterative method followed by Maj *et al.* [17]. In the present analysis, we assumed the γ -multiplicity distribution to be of the form

$$P(M) = \frac{2M + 1}{\exp\left(\frac{M - M_0}{\Delta M}\right) + 1}, \quad (2)$$

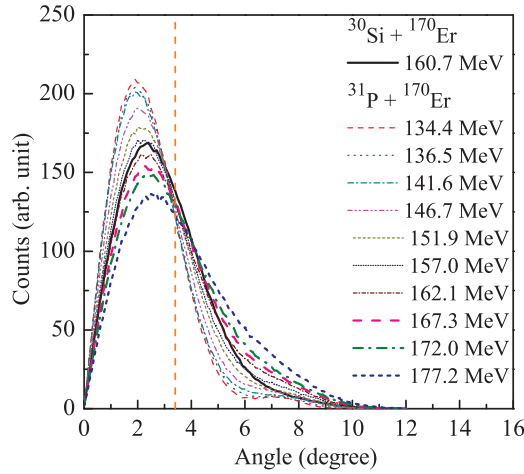


FIG. 4. (Color online) Angular distributions for $^{31}\text{P} + ^{170}\text{Er}$ at different E_{lab} calculated by TERS are shown here. The thick solid line shows angular distribution for $^{30}\text{Si} + ^{170}\text{Er}$ at $E_{\text{lab}} = 160.7$ MeV. The vertical line represents the angular acceptance of the HYRA with polar angle 3.4° .

where M_0 and ΔM are free parameters. The fold distribution $P(p)$ can then be written as

$$P(p) = \sum_{M=0}^{\infty} R(p, M)P(M). \quad (3)$$

Experimental γ -fold distributions were fitted by varying these two parameters and the best-fit values were obtained. The first 2–3 folds were contaminated with γ rays from nonfusion events. To simulate this contamination we added an extra contribution in initial folds by hand. Experimental and fitted fold distributions are shown in Fig. 6. The contamination at the lower folds, however, did not affect the values of M_0 and ΔM as the γ -fold, originating from ERs, peaked near folds 7–8. The corresponding γ -multiplicity distributions are shown in Fig. 7. An error of $\pm 10\%$ in efficiency of NaI detectors was

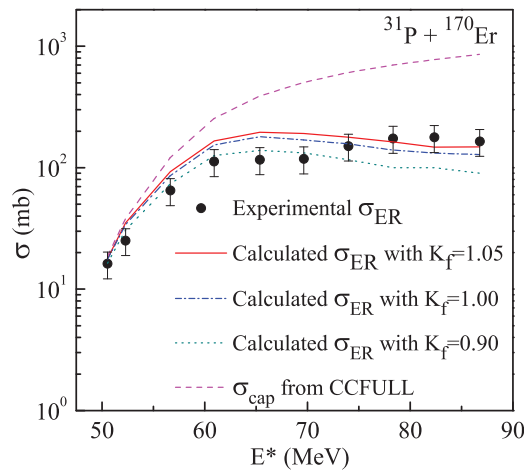


FIG. 5. (Color online) Experimental and calculated σ_{ER} for $^{31}\text{P} + ^{170}\text{Er}$ as a function of E^* . Calculated σ_{ER} with different values of K_f are denoted by different lines. Fusion cross sections (σ_{cap}), calculated using CCFULL, are also shown.

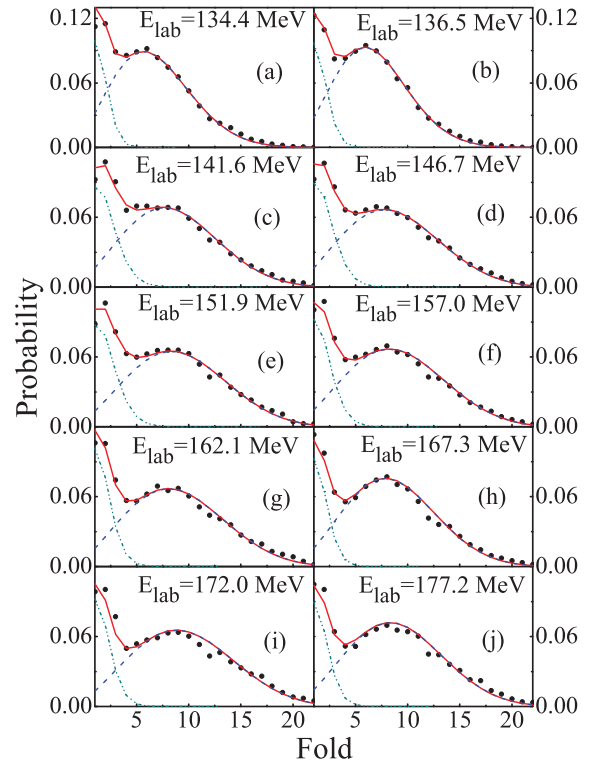


FIG. 6. (Color online) Experimental ER-gated γ -fold distributions for $^{31}\text{P} + ^{170}\text{Er}$ at different E_{lab} . Fitted γ -fold distributions are also shown. Dashed lines are fitted γ -fold for ERs and dash-dotted lines are contribution from contamination. Solid lines are total γ -fold distributions.

included in the calculation because of uncertainty in energy of detected γ rays. Details of error calculation were reported in Ref. [16].

Since the ER populations in both the reactions were quite similar, except for a few bismuth isotopes (mainly $^{194,195,196,197}\text{Bi}$), we took the average spin ($\langle \ell_{\gamma\text{ns}} \rangle$) carried away by each nonstatistical γ ray to be 1.5, the same as was considered for the system $^{30}\text{Si} + ^{170}\text{Er}$ [16]. ER spin distributions for the reaction $^{31}\text{P} + ^{170}\text{Er}$ are shown in Fig. 8.

IV. STATISTICAL MODEL CALCULATION

Statistical model calculation was performed to reproduce ER cross sections as well as the ER spin distributions. Details of the model can be found in Ref. [18]. In this calculation, partial fusion cross sections were used as input. We first carried out CCFULL [19] calculation for the system $^{30}\text{Si} + ^{170}\text{Er}$ and the parameters were adjusted to reproduce the experimental fusion cross sections (σ_{cap}), taken from Ref. [14]. The potential parameters were found to be $V_0 = 73.61$ MeV, $r_0 = 1.20$ fm, and $a_0 = 0.67$ fm. Rotational coupling for the target was included with $N = 5$ and $\beta_2 = 0.296$ [20]. For the system $^{31}\text{P} + ^{170}\text{Er}$, fusion cross sections are not available. Since $^{30}\text{Si} + ^{170}\text{Er}$ and $^{31}\text{P} + ^{170}\text{Er}$ are very similar systems and for $^{30}\text{Si} + ^{170}\text{Er}$, CCFULL could reproduce the fusion cross sections, we obtained fusion cross sections for $^{31}\text{P} + ^{170}\text{Er}$ from CCFULL calculation.

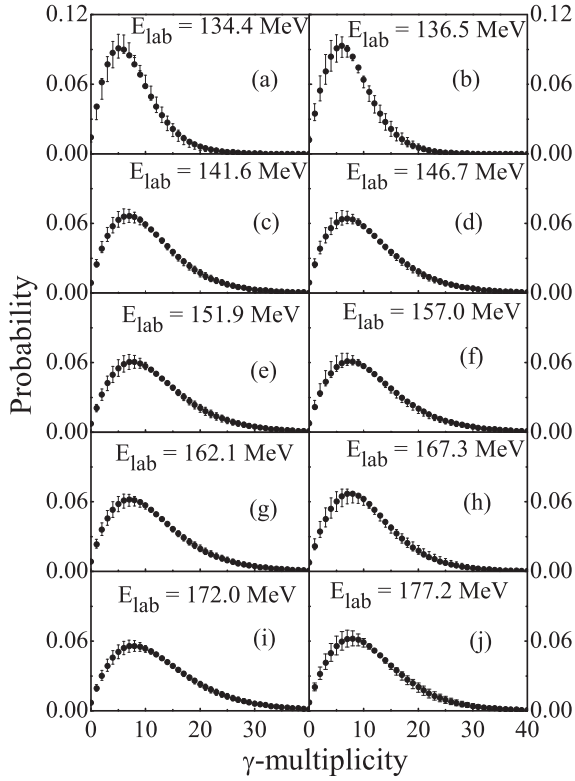


FIG. 7. ER-gated γ -multiplicity distributions for $^{31}\text{P} + ^{170}\text{Er}$ at different E_{lab} .

Some more details of the statistical model calculations were reported elsewhere [16]. It was assumed that noncompound events were absent and only CN formation and its decay were considered. Evaporation of γ rays, proton, neutron, α particle, and fission were considered to be the decay modes. Fission decay width was taken from Bohr and Wheeler [21] as

$$\Gamma_{\beta} = \frac{1}{2\pi\rho_g(E_i)} \int_0^{E_i - B_f} \rho_s(E_i - B_f - \varepsilon) d\varepsilon, \quad (4)$$

where ρ_g and ρ_s are level densities at the ground state and at the saddle point. E_i is the initial excitation energy of the CN and B_f is the fission barrier, which was obtained from the finite-range liquid drop model [22]. Level density was calculated by the equation [23]

$$\rho(E, \ell) = \frac{2\ell + 1}{12I^{\frac{3}{2}}} \sqrt{a} \frac{\exp(2\sqrt{aE})}{E^2}, \quad (5)$$

where a is the level density parameter, given by the equation [24]

$$a(E) = \bar{a} \left[1 + \frac{1 - \exp\left(-\frac{E}{E_D}\right)}{E} \Delta N \right]. \quad (6)$$

ΔN is the shell correction and E_D is the strength with which the shell correction melts away. \bar{a} is the asymptotic value which the level density parameter approaches to, with increasing energy E . Fission width is strongly dependent on B_f and a_f/a_n , a_f and a_n being the level density parameters at saddle and ground state deformations, respectively, but to compare

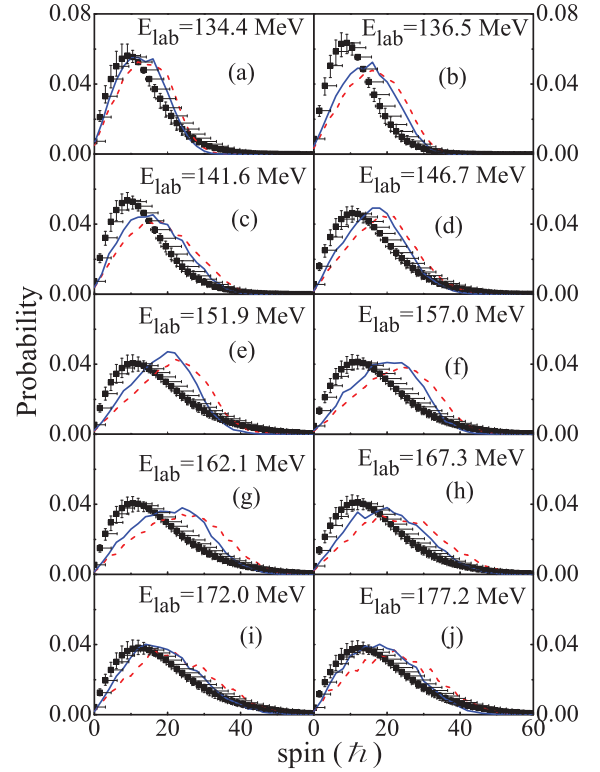


FIG. 8. (Color online) Experimental and calculated ER spin distributions for the system $^{31}\text{P} + ^{170}\text{Er}$ are shown for different E_{lab} . Solid squares are experimental ER spin distributions and solid lines are calculated ER spin distributions. Calculated spin distributions of CN which produced ER (i.e., ER-gated CN spin distribution) are also shown by dashed lines.

with the experimental σ_{ER} only B_f was varied. In Fig. 9, σ_{ER} for $^{30}\text{Si} + ^{170}\text{Er}$ are shown along with statistical model calculations and in Fig. 5 the experimental and calculated σ_{ER} for $^{31}\text{P} + ^{170}\text{Er}$ are presented. The same statistical model

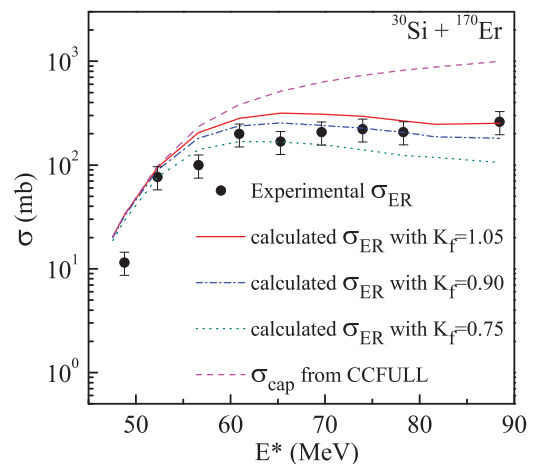


FIG. 9. (Color online) Experimental and calculated σ_{ER} for $^{30}\text{Si} + ^{170}\text{Er}$ as a function of E^* . Calculated σ_{ER} with different values of K_f are denoted by different lines. Fusion cross sections (σ_{cap}), calculated using CCFULL, are also shown.

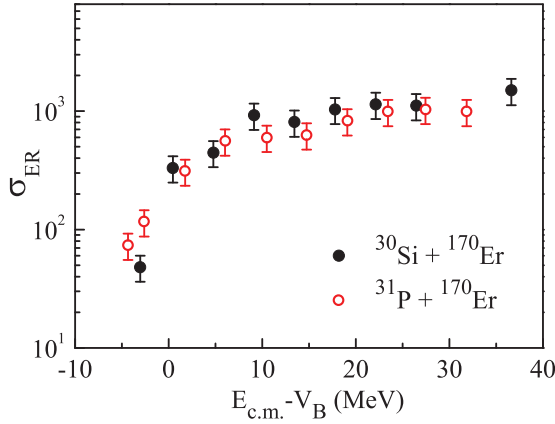


FIG. 10. (Color online) $\tilde{\sigma}_{ER}$ for systems $^{30}\text{Si} + ^{170}\text{Er}$ and $^{31}\text{P} + ^{170}\text{Er}$ as a function of energy excess over the Coulomb barrier, $E_{c.m.} - V_B$, where $E_{c.m.}$ is the center-of-mass energy.

calculation was used to obtain the ER spin distributions. When a particle is evaporated from the CN, the spin of the particle is subtracted to obtain the spin of the daughter nuclei. If spin of the evaporated particle and parent nuclei are ℓ_v and ℓ_p and that of the daughter nuclei is ℓ_d , then

$$|\ell_p - \ell_v| \leq \ell_d \leq |\ell_p + \ell_v|. \quad (7)$$

The probability of a particular value of ℓ_d is given by

$$\frac{(2\ell_d + 1) \exp\left[2\sqrt{a_d}\left(E_{\text{tot}} - \frac{(\ell_d h)^2}{2I_d}\right)\right]}{\int_{|\ell_p - \ell_v|}^{\ell_p + \ell_v} (2\ell_d + 1) \exp\left[2\sqrt{a_d}\left(E_{\text{tot}} - \frac{(\ell_d h)^2}{2I_d}\right)\right] d\ell_d}. \quad (8)$$

The spin of the evaporated particle, ℓ_v , was obtained from a sampling over the range from 0 to the maximum angular momentum that can be carried away by the evaporated particle. The experimental and calculated ER spin distributions for the system $^{31}\text{P} + ^{170}\text{Er}$ are shown in Fig. 8.

V. RESULTS AND DISCUSSION

The measured reduced ER cross sections ($\tilde{\sigma}_{ER}$) for the systems $^{30}\text{Si} + ^{170}\text{Er}$ and $^{31}\text{P} + ^{170}\text{Er}$ are plotted in Fig. 10, where the reduced cross sections are obtained as $\tilde{\sigma}_{ER} = \sigma_{ER}/(\pi\bar{\lambda}^2)$, $\bar{\lambda}$ being the reduced de Broglie wavelength of entrance channel relative motion. Both sets of $\tilde{\sigma}_{ER}$ match within experimental error. To match experimental σ_{ER} with calculated values, we had to reduce B_f in statistical model calculation. The scaling factor (K_f) of fission barrier in the case of $^{30}\text{Si} + ^{170}\text{Er}$ varied from 0.75 to 1.05 and that for $^{31}\text{P} + ^{170}\text{Er}$ varied from 0.90 to 1.05. Thus reduction in B_f by similar amounts could explain experimental σ_{ER} for both the systems. In Fig. 11, we show the best-fit values of K_f as a function of excitation energy for both systems. The values are slightly less in the case of $^{30}\text{Si} + ^{170}\text{Er}$ but differences are within the range of error.

We next show in Fig. 12 the γ -multiplicity distributions for the two systems at nearly the same excitation energies. It

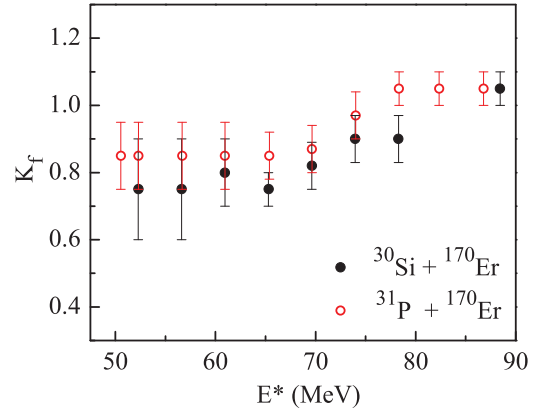


FIG. 11. (Color online) Best-fit values of K_f as a function of E^* for $^{30}\text{Si} + ^{170}\text{Er}$ and $^{31}\text{P} + ^{170}\text{Er}$.

reveals that the distributions are quite similar. This fact is also reflected in Fig. 13 where moments of γ -multiplicity distributions are compared for these two systems. No difference is observed in mean and variance values. Skewness for the two systems are also very similar except at a few higher energy points where $^{31}\text{P} + ^{170}\text{Er}$ shows slightly higher values.

When experimental and calculated spin distributions were compared (see Fig. 8), the experimental spin distributions peaked at lower values than the calculated spin distributions for $^{31}\text{P} + ^{170}\text{Er}$. A similar trend was observed in the case of $^{30}\text{Si} + ^{170}\text{Er}$ as well, which could be due to the presence of noncompound fission [16]. In statistical model calculation we considered only complete fusion between target and projectile after capture. The possibility of noncompound fission was neglected. The presence of noncompound fission in these reactions is expected to reduce σ_{ER} in both the systems by a similar amount as the entrance channel mass asymmetry, fissility, and excitation energy are comparable. Spin distributions in both cases are also expected to be similar.

The process of conversion from γ -multiplicity distribution to spin distribution is associated with a large error and hence any small difference in spin distributions of the

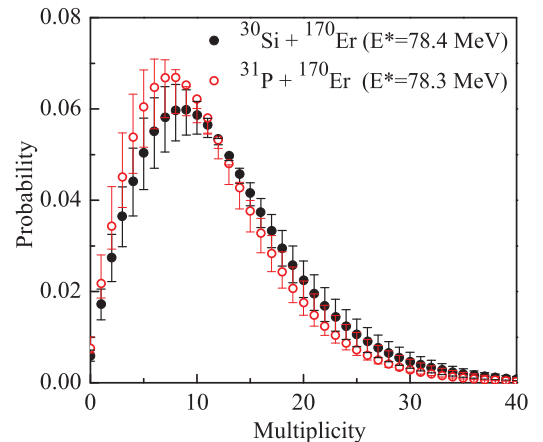


FIG. 12. (Color online) ER-gated γ -multiplicity distributions for $^{30}\text{Si} + ^{170}\text{Er}$ and $^{31}\text{P} + ^{170}\text{Er}$ at similar E^* .

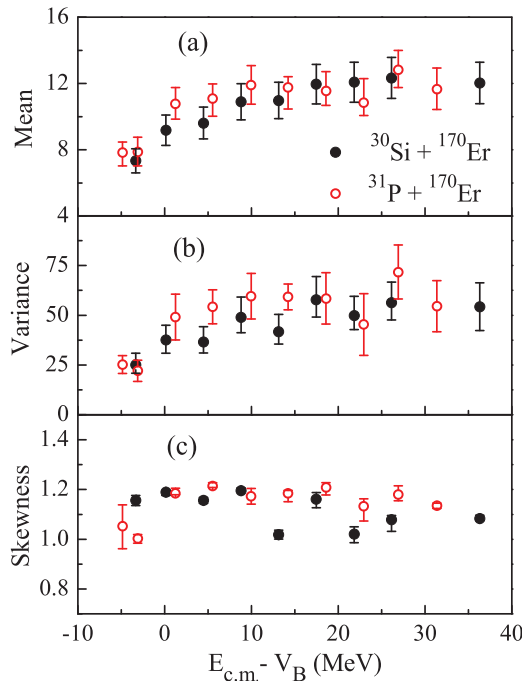


FIG. 13. (Color online) The first three moments of γ -multiplicity distributions for $^{30}\text{Si} + ^{170}\text{Er}$ and $^{31}\text{P} + ^{170}\text{Er}$ as a function of energy excess over the Coulomb barrier.

two systems is difficult to observe [16]. However, in the present case, the ERs produced in both the reactions are quite similar. So we have taken ($\ell_{\gamma\text{ns}}$) to be the same for both the systems. This allowed us to compare directly the

γ -multiplicity distributions and we could avoid the large errors arising due to conversion from γ -multiplicity distribution to spin distribution. The error involved in finding γ -multiplicity distribution from γ -fold distribution comes mainly from the uncertainty in efficiency of γ detectors.

VI. CONCLUSION

σ_{ER} and ER-gated γ -multiplicity distribution were measured for the system $^{31}\text{P} + ^{170}\text{Er}$ over a wide range of E_{lab} . Results were compared for the reactions $^{30}\text{Si} + ^{170}\text{Er}$ and $^{31}\text{P} + ^{170}\text{Er}$, forming CN ^{200}Pb ($Z = 82$) and ^{201}Bi ($Z = 83$), respectively. Measured σ_{ER} for these two systems were compared with statistical model calculations. Similar statistical model parameters could reproduce the data for both the reactions. Moments of γ -multiplicity distributions for the two systems were also compared and found to be quite similar. In conclusion, no significant effect of CN proton shell closure on survival of ERs against fission was observed by comparing the two systems. More measurements of σ_{ER} and comparison between more systems forming CN/ER in the vicinity of $Z = 82$ may elucidate the stabilizing effect of the proton shell closure further.

ACKNOWLEDGMENTS

The authors are thankful to the accelerator staff of IUAC for providing good quality beams and S. R. Abhilash for his cooperation during target fabrication. One of the authors (G.M.) acknowledges financial support from the Council of Scientific and Industrial Research (CSIR), Government of India.

- [1] A. Sobczewski, F. Gareev, and B. Kalinkin, *Phys. Lett.* **22**, 500 (1966).
- [2] Y. Oganessian, *J. Phys. G: Nucl. Part. Phys.* **34**, R165 (2007).
- [3] S. Hofmann and G. Müntzenberg, *Rev. Mod. Phys.* **72**, 733 (2000).
- [4] K. Satou, H. Ikezoe, S. Mitsuoka, K. Nishio, and S. C. Jeong, *Phys. Rev. C* **65**, 054602 (2002).
- [5] A. Shrivastava, S. Kailas, A. Chatterjee, A. M. Samant, A. Navin, P. Singh, and B. S. Tomar, *Phys. Rev. Lett.* **82**, 699 (1999).
- [6] K. Mahata, S. Kailas, A. Shrivastava, A. Chatterjee, P. Singh, S. Santra, and B. S. Tomar, *Phys. Rev. C* **65**, 034613 (2002).
- [7] S. Nath, P. V. M. Rao, S. Pal, J. Gehlot, E. Prasad, G. Mohanto, S. Kalkal, J. Sadhukhan, P. D. Shidling, K. S. Golda *et al.*, *Phys. Rev. C* **81**, 064601 (2010).
- [8] G. Mohanto, S. R. Abhilash, D. Kabiraj, N. Madhavan, and R. K. Bhowmik, *J. Radioanal. Nucl. Chem.* **297** (2013), doi: 10.1007/s10967-013-2640-6.
- [9] N. Madhavan, S. Nath, T. Varughese, J. Gehlot, A. Jhingan, P. Sugathan, A. K. Sinha, R. Singh, K. M. Varier, M. C. Radhakrishna *et al.*, *Pramana J. Phys.* **75**, 317 (2010).
- [10] S. Nath, A Monte Carlo code to model ion transport in dilute gas medium (unpublished).
- [11] G. A. Kumar, I. Mazumdar, and D. Gothe, IEEE Nuclear Science Symposium Conference Record, p. 1640 (2008).
- [12] G. A. Kumar, I. Mazumdar, and D. Gothe, *Nucl. Instrum. Methods Phys. Res., Sect. A* **76**, 611 (2009).
- [13] E. Prasad, K. M. Varier, N. Madhavan, S. Nath, J. Gehlot, S. Kalkal, J. Sadhukhan, G. Mohanto, P. Sugathan, A. Jhingan *et al.*, *Phys. Rev. C* **84**, 064606 (2011).
- [14] D. Hinde, J. Leigh, J. Newton, W. Galster, and S. Sie, *Nucl. Phys. A* **385**, 109 (1982).
- [15] S. Nath, *Comput. Phys. Commun.* **180**, 2392 (2009).
- [16] G. Mohanto, N. Madhavan, S. Nath, J. Sadhukhan, J. Gehlot, I. Mazumdar, M. B. Naik, E. Prasad, I. Mukul, T. Varughese *et al.*, *Nucl. Phys. A* **890-891**, 62 (2012).
- [17] A. Maj, J. J. Gaardhaje, A. Atac, S. Mitarai, J. Nyberg, A. Virtanen, A. Bracco, F. Camera, B. Million, and M. Pignanelli, *Nucl. Phys. A* **571**, 185 (1994).
- [18] G. Chaudhuri and S. Pal, *Phys. Rev. C* **65**, 054612 (2002).
- [19] K. Hagino, N. Rowley, and A. Kruppa, *Comput. Phys. Commun.* **123**, 143 (1999).
- [20] P. Möller, J. R. Nix, W. D. Myers, and W. J. Swiatecki, *At. Data Nucl. Data Tables* **59**, 185 (1995).
- [21] N. Bohr and J. Wheeler, *Phys. Rev.* **56**, 426 (1939).
- [22] A. J. Sierk, *Phys. Rev. C* **33**, 2039 (1986).
- [23] A. Bohr and B. Mottelson, *Nuclear Structure* **1**, 426 (1969).
- [24] A. Ignatyuk, M. Itkis, V. Okolovich, G. Smirenkin, and A. Tishin, *Sov. J. Nucl. Phys.* **21**, 255 (1975).